



Effect of Heat and Mass Transfer over Mixed Convective Hybrid Nanofluids past an Exponentially Stretching Sheet

P. Chandrakala^{1,*}, V. Srinivasa Rao¹

¹ Department of Mathematics, Anurag University, Hyderabad, Telangana, India

ARTICLE INFO

Article history:

Received 22 July 2023

Received in revised form 20 August 2023

Accepted 18 September 2023

Available online 12 December 2023

Keywords:

Heat Transfer; Mass Transfer; Mixed convection; Slip conditions

ABSTRACT

The presented study investigates the heat and mass transfer characteristics of hybrid nanofluid flow past an exponentially enlarging sheet, featuring both heat source and sink effects. A distinctive aspect of this work lies in its examination of slip conditions to understand the flow behavior of hybrid nanofluids. The nanofluid itself consists of a blend of copper (Cu) and metal oxide (Al₂O₃) nanoparticles suspended in blood, which serves as the base fluid. This choice of nanofluid composition is noteworthy due to its potential impact on enhancing heat and mass transfer processes. Similarity conversion technique is applied that effectively transforms the partial differential equations (PDEs) governing the system into a set of ordinary differential equations (ODEs). The utilization of tables and graphs aids in conveying the influence of various embedded parameters on the obtained results. This graphical representation of parameter effects is a distinctive feature of the study, facilitating a clearer understanding of the relationships between different variables. In the concluding remarks, the study's outcomes highlight several distinctive findings. Firstly, an increase in the heat-generating parameter leads to elevated temperature distribution along the expanding sheet. Secondly, the introduction of a magnetic parameter is found to dampen the velocity of the nanofluids, which presents an interesting avenue for exploration in terms of flow control. Thirdly, the concentration profile of the nanofluids experiences a decline as the Schmidt number, a dimensionless quantity representing the ratio of momentum diffusivity to mass diffusivity, increases. It concluded that the heat and mass transfer rate is greatly enhanced by the addition of copper and aluminium oxide. This observation is a unique contribution to the understanding of heat and mass transfer behavior in such systems. The significance of this research extends to various applications, particularly in the realms of chemical engineering, environmental remediation processes, and solar thermal systems.

1. Introduction

In our modern era, the utilization of machinery and advanced technology closely parallels the fields of civil, mechanical, and engineering. It is widely recognized that machinery generates heat during its operation. As a consequence of this increased heat production, machinery becomes less efficient and consumes more energy. To address this issue, various technologies and methods have been developed, many of which involve the use of different fluid types such as water, minerals, organic compounds (such as ethylene glycol, refrigerants, and tri-ethylene glycol), bio-based fluids, and herbal oils. These fluid mediums are employed to mitigate the generation of excess heat within

* Corresponding author.

E-mail address: chandrakalapanguluri@gmail.com (P. Chandrakala)

operating machinery. Scientific environments such as hydroelectric, thermal and nuclear power plants have extensively employed these fluids. However, conventional fluids have certain limitations when used as coolants due to their relatively low heat capacity. To overcome this limitation, ground-breaking scientists Choi and Eastman proposed a novel concept [1]. By incorporating metal oxides and metal alloys into common fluids, the heat capacity can be significantly enhanced. This innovative approach makes the fluids more resistant to high temperatures compared to their common counterparts. The research suggested that the particle size should be decreased in order to maximize the heat capacity of the suspension and decrease the likelihood of particle agglomeration in the base fluids. The common fluids in the suspensions are referred to as base fluids, while the solid particles are known as nanoparticles.

A fundamental thermo-fluidic phenomenon recognized as mixed convection arises from the harmonious convergence of forced and natural convection dynamics. Convection, at its essence, signifies the intricate transfer of thermal energy from a region of higher temperature to one of lower temperature. In the realm of free convection, this intricate energy exchange manifests as a result of density disparities, whereas in forced convection, an extrinsic impetus propels the mixing motion. The mixture of these two distinct convective modes finds expression in the term 'mixed convection'. In the unfolding narrative of fluid dynamics, the investigation of mixed convection boundary layer flows emerges as pivotal, poised to shape the contours of technological advancement and scientific understanding. Furthermore, pronounced thermal sources (generation) or sinks (absorption) influences [22] can manifest due to notable temperature gradients existing between the interface and the encompassing fluid medium. A recent investigation conducted by Ramzan *et al.*, [2] delved into the intricate interplay of Fourier's and Fick's laws, Newtonian heating, and the application of magnetohydrodynamics (MHD) to a dusty Casson nanofluid flowing through a cylinder undergoing stretching. In one study, a hybrid nanofluid made up of water and Ag-CuO nanoparticles was explored by Hayat and Nadeem [3] to observe its behavior in a three-dimensional rotational flow situation. On the other hand, Waini *et al.*, [4–6] explored the distinctive features of flow over a stretching surface in a hybrid nanofluid and conducted a temporal stability analysis.

The effect of heat transfer in hybrid nanofluids [7–15] in different geometries is explained by different authors. Chamkha *et al.*, [11] explored the heat transfer enhancement properties of a water-based nanofluid containing Al_2O_3 and Cu nanoparticles in a semi-circular cavity. However, a thorough analysis of the existing literature reveals that the flow across a moving wedge included in the hybrid nanofluid was not taken into account. Various investigations on hybrid nanofluids in different geometry are Umar *et al.*, [16] explored the numerical dual solutions of the MHD stagnation point flow induced by hybrid nanofluids towards a porous moving inclined flat plate with mixed convection and thermal radiation. The impact of hybrid nanoparticles on different physical quantities in a Cu- Fe_3O_4 /ethylene glycol-based hybrid nanofluid is associated with a steady and fully developed natural convective flow over a stretching surface [17]. The flow and heat transfer effects of MHD dusty hybrid nanofluids over a shrinking sheet are studied by Nepal Chandra Roy *et al.*, [18]. Recently, many researchers investigated motivating results about hybrid nanofluids, concentrating on alumina and copper as the hybrid nanoparticles, with different arrangements of the parameters, as exposed by Najiyah Safwa Khashi'ie *et al.*, [19] and Sulochana *et al.*, [20]. In order to explore the boundary layer properties of a permeable plate immersed in a porous medium, Bestman [26] considered binary chemical reactions dependent on the activation energy some decades ago.

The above review shows that no research has been conducted yet on the topic of heat and mass transfer in hybrid nanofluids over stretching sheets. It has been endeavored with less attention, though it has many applications in various engineering, biological, and industrial contexts. This distinctive nanofluid, comprising $\text{CuO}/\text{Al}_2\text{O}_3$ nanoparticles suspended in a blood base fluid, remains

unexplored in the context of its flow past an exponentially expanding sheet while encountering a heat source. Hence, the aim of this investigation is to scrutinize the heat and mass transfer characteristics of mixed convective hybrid nanofluids, subject to the influence of a magnetic field, flowing over an exponentially stretching sheet while accommodating velocity, thermal, and concentration slip conditions.

2. Mathematical Formulation

In this present study, we consider the steady, laminar, two-dimensional, thermally radiated mixed convection magnetohydrodynamic (MHD) hybrid nanofluid flow past an exponentially stretching sheet. Figure 1, depicts the geometry of the problem, with u and v the components of velocity in x and y directions for the flow, where x and y are Cartesian coordinates with the x -axis parallel to the plate, where y -axis is perpendicular to the plate. The fluid's surface velocity is considered as $u_w(x) = ce^{-\frac{x}{L}}$, and the wall's mass transfer velocity is expressed as $v_w(x) = v_0 e^{x/2L}$, while $v_0 < 0$ and $v_0 > 0$ indicates mass suction and injection respectively. Additionally, the constant for stretching is represented by $\lambda > 0$. 'T' indicates temperature, $T_w = T_\infty + T_0 e^{x/2L}$ is differing temperature with constant T_0 and $q = q_0 e^{x/L}$ is heat generation rate constant.

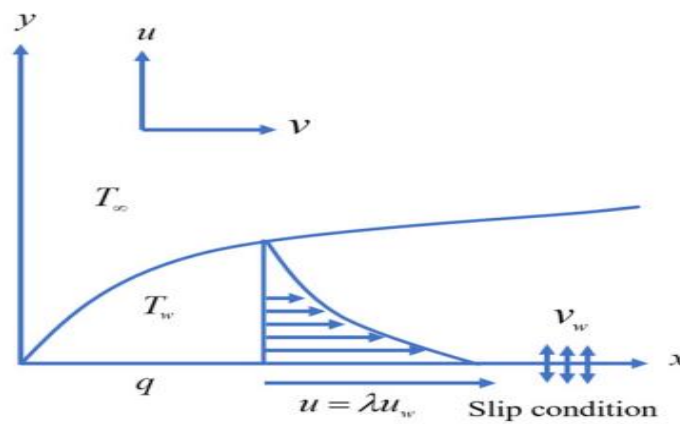


Fig. 1. Physical model of the problem for stretching sheet

As a result, the following equations are for continuity, momentum, energy and chemical reaction:

$$u \frac{\partial u}{\partial x} + v \frac{\partial v}{\partial y} = 0 \quad (1)$$

$$u \frac{\partial u}{\partial x} + v \frac{\partial u}{\partial y} = \frac{\mu_{hnf}}{\rho_{hnf}} \frac{\partial^2 u}{\partial y^2} - \frac{\sigma_{hnf} B_0^2 u}{\rho_{hnf}} + \frac{(\rho\beta)_{hnf}}{(\rho\beta)_{hnf}} (T - T_\infty) g + \frac{(\rho\beta)_{hnf}}{(\rho\beta)_{hnf}} (C - C_\infty) g \quad (2)$$

$$u \frac{\partial T}{\partial x} + v \frac{\partial T}{\partial y} = \frac{k_{hnf}}{(\rho c_p)_{hnf}} \frac{\partial^2 T}{\partial y^2} + \frac{q}{(\rho c_p)_{hnf}} (T - T_\infty) \quad (3)$$

$$u \frac{\partial C}{\partial x} + v \frac{\partial C}{\partial y} = D_B \frac{\partial^2 C}{\partial y^2} - K_1 (C - C_\infty) \quad (4)$$

The boundary conditions that are appropriate for this flow are;

$$\left. \begin{aligned} u &= u_w(x)\lambda + A_1 \frac{\mu_{hnf}}{\rho_{hnf}} \frac{\partial u}{\partial y} \\ v &= v_w \quad T = T_w(x) + B_1 \frac{\partial T}{\partial y}, \quad C = C_w(x) + C_1 \frac{\partial C}{\partial y} \quad \text{at } y = 0 \end{aligned} \right\} \quad (5)$$

$$u \rightarrow 0, \quad v \rightarrow 0, \quad T \rightarrow T_\infty, \quad C \rightarrow C_\infty \quad \text{as } y \rightarrow \infty \quad (6)$$

Slip factors for velocity, temperature, and concentration are designated as A_1 , B_1 , and C_1 , respectively. The investigations carried out by Tayebi *et al.*, [27], Takabi *et al.*, [28], and Oztop *et al.*, [29] are based on the correlation of the fluid's physical properties, including the hybrid nanofluid. These correlations are presented in Tables 1 and 2, presenting the base fluid, alumina, and copper nanoparticles (s_1 , s_2) and their interactions with the hybrid nanofluid's thermo-physical characteristics. Copper and alumina volume fraction parameters of nanoparticles are represented by ϕ_{s1} and ϕ_{s2} , respectively.

Table 1
 Hybrid nanofluid physical properties

Properties	Hybrid nanofluid correlations
Density	$\rho_{hnf} = \rho_{s1}\phi_{s1} + \rho_{s2}\phi_{s2} + \rho_f (1 - \phi_{hnf})$ Where $\phi_{hnf} = \phi_{s1} + \phi_{s2}$
Heat capacity	$(\rho c_p)_{hnf} = (\rho c_p)_{s1}\phi_{s1} + (\rho c_p)_{s2}\phi_{s2} + (\rho c_p) (1 - \phi_{hnf})$
Dynamic conductivity	$\frac{\mu_{hnf}}{\rho_{hnf}} = 1 / (1 - \phi_{hnf})^{2.5}$
Thermal conductivity	$\frac{\mu_{hnf}}{\rho_{hnf}} = \left[\frac{2k_f + \{(\phi_{s1}k_{s1} + \phi_{s2}k_{s2}) / \phi_{hnf}\} + 2(\phi_{s1}k_{s1} + \phi_{s2}k_{s2}) - 2\phi_{hnf}}{2k_f - \{(\phi_{s1}k_{s1} + \phi_{s2}k_{s2})\} + (\phi_{s1}k_{s1} + \frac{\phi_{s2}k_{s2}}{\phi_{hnf}}) + \phi_{hnf}k_f} \right]$

Table 2
 Thermal physical properties

Physical Properties	Blood	Al ₂ O ₃	Cu
$\rho \left(\frac{kg}{m^3} \right)$	1053	3970	8933
C_p (J/kgK)	3594	765	385
K(W/mk)	0.492	40	400

To simplify the governing Eq. (2) - Eq. (4), we apply the following transformations:

$$\psi = e^{x/2L} \sqrt{2\nu_f L c} f(\eta), u = \frac{\partial \psi}{\partial y}, v = -\frac{\partial \psi}{\partial x}, \eta = ye^{x/2L} \sqrt{\frac{c}{2\nu_f L}}, \theta(\eta) = \frac{T - T_\infty}{T_w - T_\infty}, \phi(\eta) = \frac{C - C_\infty}{C_w - C_\infty} \quad (7)$$

$$u = ce^{x/L} f'(\eta), v = -\sqrt{\nu_f c / 2Le^{x/L}} \{ \eta f'(\eta) + f(\eta) \}$$

These variables satisfy Eq. (1) and lead to the transformation of Eq. (2), (3) and (4).

$$\begin{aligned} & \left(\begin{array}{c} \left(\frac{\mu_{hnf}}{\mu_f} \right) \\ \left(\frac{\rho_{hnf}}{\rho_f} \right) \end{array} \right) f''' + ff'' - 2f'^2 - \left(\begin{array}{c} \left(\frac{\sigma_{hnf}}{\sigma_f} \right) \\ \left(\frac{\rho_{hnf}}{\rho_f} \right) \end{array} \right) Mf' + 2Gr \left(\begin{array}{c} \left(\frac{(\rho\beta)_{hnf}}{\rho_f} \right) \\ \left(\frac{\rho_{hnf}}{\rho_f} \right) \end{array} \right) \theta \\ & + 2Gc \left(\begin{array}{c} \left(\frac{(\rho\beta)_{hnf}}{\rho_f} \right) \\ \left(\frac{\rho_{hnf}}{\rho_f} \right) \end{array} \right) \Phi = 0 \end{aligned} \quad (8)$$

$$\frac{\left\{ \frac{k_{hnf}}{k_f} \right\} \theta''}{Pr} - \frac{(\rho c_p)_{hnf}}{(\rho c_p)_f} (4f'\theta - \theta'f) + 2Q\theta = 0 \quad (9)$$

$$\phi'' - Sc(4f'\phi - f\phi') - 2Sc.Kr.\phi = 0 \quad (10)$$

The modified boundary conditions corresponding to the transformation are then

$$f(0) = s, f'(0) = \lambda + cf'', f'(\infty) = 0, \theta(0) = 1 + B\theta'(0), \theta(\infty) = 0, \phi(0) = 1 + C\phi'(0), \phi(\infty) = 0 \quad (11)$$

Where

$$\left\{ \begin{array}{l} M = \frac{\sigma B_0^2 e^{-x/L}}{c\rho_f}, Pr = \frac{\nu_f}{k_f} = \frac{(\nu\rho C_p)_f}{k_f}, \theta_w = \frac{T_w}{T_\infty}, Gr = \frac{g\beta_f T_0 L}{c^2}, Gc = \frac{g\beta_f C_0 L}{c^2}, S_c = \frac{\nu_f}{D_m} \\ K_r = \frac{K_1 L}{C} e^{-x/L}, Q = qL / c (\rho c_p)_f \end{array} \right.$$

$A = A_1 \frac{\mu_{hmf}}{\rho_{hmf}} e^{x/2L} \sqrt{\frac{c}{2\nu_f L}}$ show the velocity slip parameter, $B = B_1 e^{x/2L} \sqrt{\frac{c}{2\nu_f L}}$ denotes thermal slip parameter, $C = C_1 e^{x/2L} \sqrt{\frac{c}{2\nu_f L}}$ denotes the concentration slip parameter, and $S = -v_0 / \sqrt{2\nu_f c/2L}$ represents the mass transfer parameter of the wall, in which $S > 0$ ($v_0 < 0$) and $S < 0$ ($v_0 > 0$) are mass suction and injection respectively. The Nusselt number (Nu_x) and the skin friction coefficient (C_f), which are the two primary physical characteristics of interest, are computed as in Ref. [9].

$$Cf_x = \frac{\mu_{hmf}}{\rho_{hmf} (u_w)^2} \left(\frac{\partial u}{\partial y} \right)_{y=0},$$

$$Nu_x = -\frac{(-2L)k_{hmf}}{k_f (T_w - T_\infty)} \left(\frac{\partial T}{\partial y} \right)_{y=0}, Sh_x = -\frac{(-2L)k_{hmf}}{k_f (C_w - C_\infty)} \left(\frac{\partial C}{\partial y} \right)_{y=0} \quad (12)$$

The coefficient of skin friction, the Nusselt number and the Sherwood number are represented in their respective non-dimensional configurations.

$$Re_x^{1/2} C_f = \frac{\mu_{hmf}}{\mu_f} f''(0), Re_x^{-1/2} C_f = -\left(\frac{\mu_{hmf}}{\mu_f}\right)\theta'(0),$$

$$Re_x^{-1/2} Sh_x = -\frac{k_{hmf}}{k_f} \phi'(0) \quad (13)$$

3. Solution Procedure using Shooting Method

Many researchers regularly use the Shooting approach [30] to find solutions to such problems [21–25] for different values of various parameters, was used to numerically solve the system of nonlinear ordinary differential equations (ODEs) (Eq. (8)–(10)) and the corresponding boundary conditions Eq. (11). For obtaining a result with an accuracy of six decimal places, the step size is chosen as a convergence criterion.

We denote f by y_1 , θ by y_4 and ϕ by y_6 for converting the boundary value problem Eq. (8)-(10) to the following initial value problem of 7 first order ordinary differential equations.

$$\begin{aligned}
 y_1' &= y_2, & y_1(0) &= s, \\
 y_2' &= y_3, & y_2(0) &= \lambda + A y_3, \\
 \left(\begin{array}{c} \frac{\mu_{hmf}}{\mu_f} \\ \frac{\rho_{hmf}}{\rho_f} \end{array} \right) y_3' &= 2y_2^2 + \left(\begin{array}{c} \frac{\sigma_{hmf}}{\sigma_f} \\ \frac{\rho_{hmf}}{\rho_f} \end{array} \right) M \cdot y_2 - 2Gr \left(\begin{array}{c} \frac{\sigma_{hmf}}{\sigma_f} \\ \frac{\rho_{hmf}}{\rho_f} \end{array} \right) y_4 - 2Gc \left(\begin{array}{c} \frac{\sigma_{hmf}}{\sigma_f} \\ \frac{\rho_{hmf}}{\rho_f} \end{array} \right) y_6, & y_3(0) &= s_1 \\
 y_4' &= y_5, & y_4(0) &= 1 + B y_5(0), \\
 \frac{\left\{ \begin{array}{c} k_{hmf} \\ k_f \end{array} \right\}}{Pr} y_5' &= \frac{(\rho c_p)_{hmf}}{(\rho c_p)_f} (4y_2 y_4 - y_5 y_1) - 2Q \cdot y, & y_5(0) &= s_2, \\
 y_6' &= y_7, & y_6(0) &= 1 + C y_7(0), \\
 y_7' &= 2Sc \cdot Kr \cdot y_6 - Sc \{ 4y_1 y_7 - y_6 y_1 \}, & y_7(0) &= s_3
 \end{aligned}$$

To solve the above initial value problem arising in the shooting method, Runge Kutta method of order four is used.

4. Results & Discussions

Figures 2–4 show how the velocity slip parameter A impacts the velocity, temperature, and concentration curves. It depicts how the slip parameter impacts temperature and velocity distributions significantly. This shows that the temperature and velocity profiles rise together with the value of the velocity slip parameter A. Figures 3 and 4 also show how the slip parameter an impacts the rates of mass and heat transfer. It can be shown that decreasing the values of a results in decreased rates of mass and heat transmission.

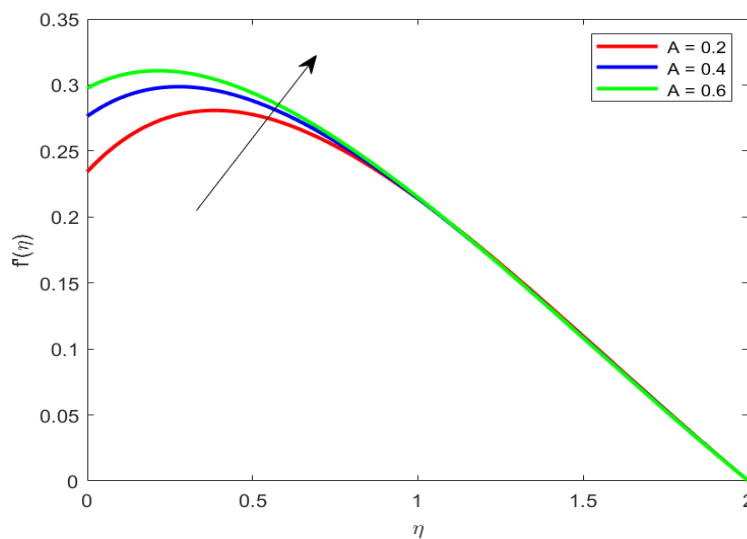


Fig. 2. Variations in $f'(\eta)$ against A

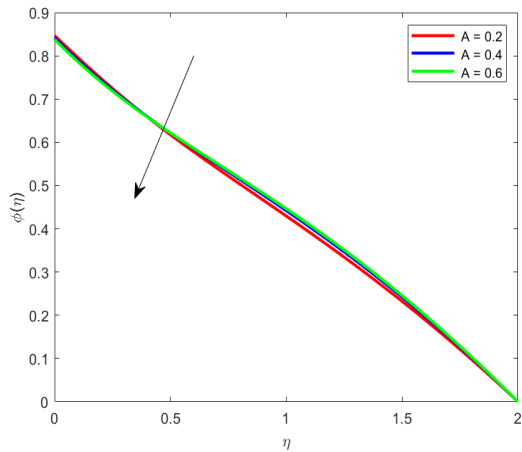


Fig. 3. Variations in $\theta(\eta)$ against A

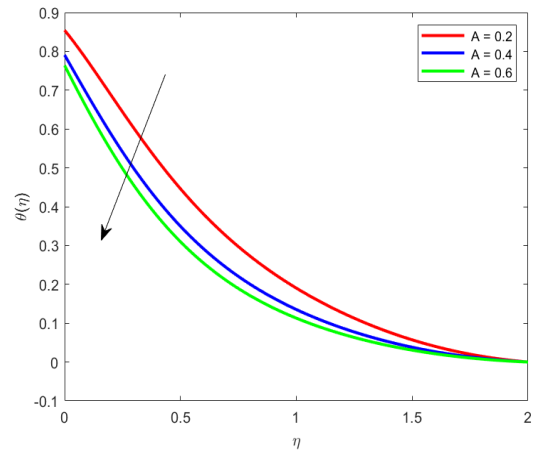


Fig. 4. Variations in $\phi(\eta)$ against A

Figures 5, 6, and 7 shows the sway of the thermal slip parameter B on the temperature profile, concentration profile, and velocity profile. It has been found that dropping the thermal slip parameter B's value, results in a decrease in both the temperature profile and velocity profile. But as the value of B grows, the concentration profile does too.

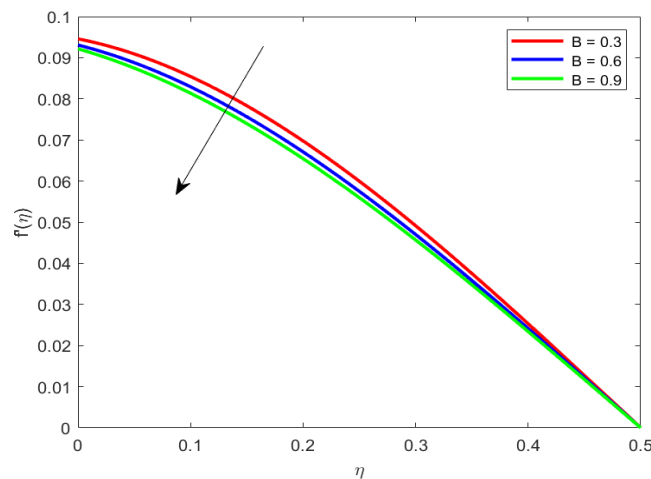


Fig. 5. Variations in $f'(\eta)$ against B

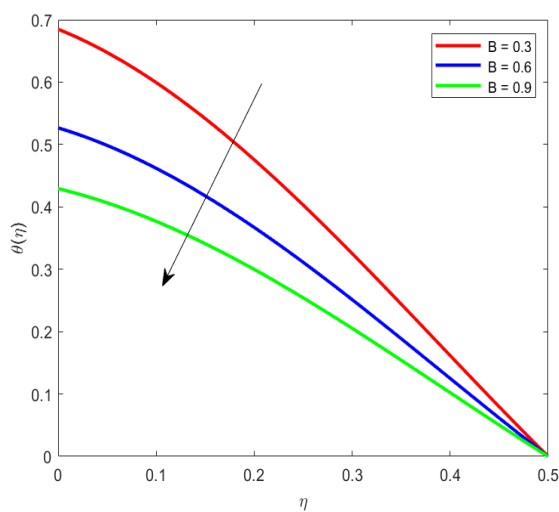


Fig. 6. Variations in $\theta(\eta)$ against B

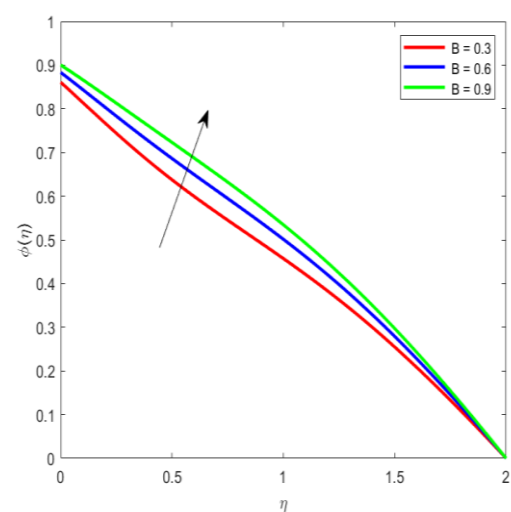


Fig. 7. Variations in $\phi(\eta)$ against B

The velocity profile $f'(\eta)$, temperature profile, and concentration profile are all altered by the concentration slip parameter C , as seen in figures 8, 9, and 10 accordingly. When the concentration slip parameter C is increased, both the velocity profile $f'(\eta)$ and the concentration profile perform worse; however, the temperature profile performs better when C is increased.

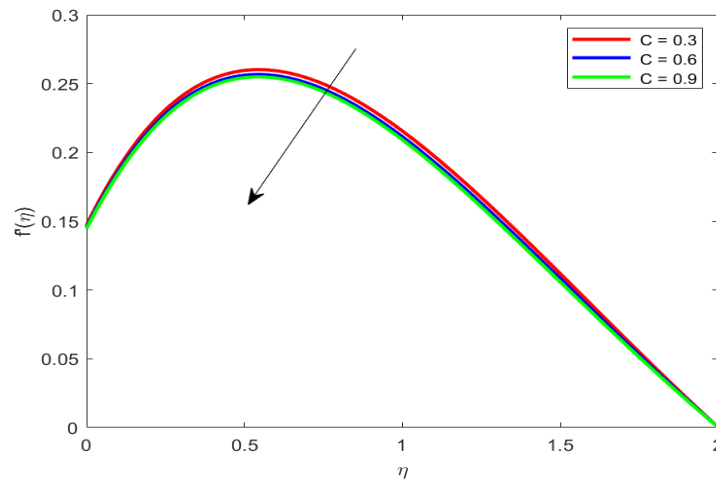


Fig. 8. Variations in $f'(\eta)$ against C

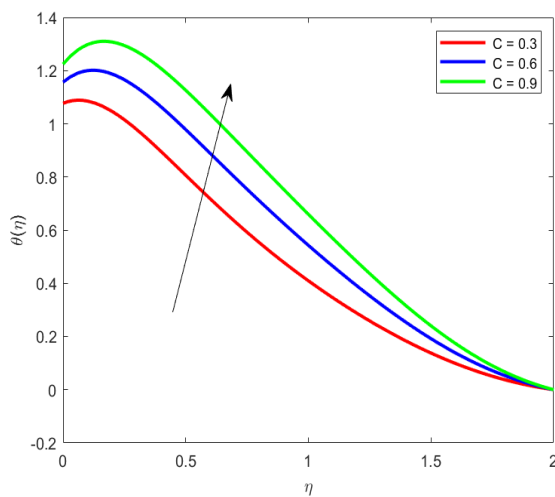


Fig. 9. Variations in $\theta(\eta)$ against C

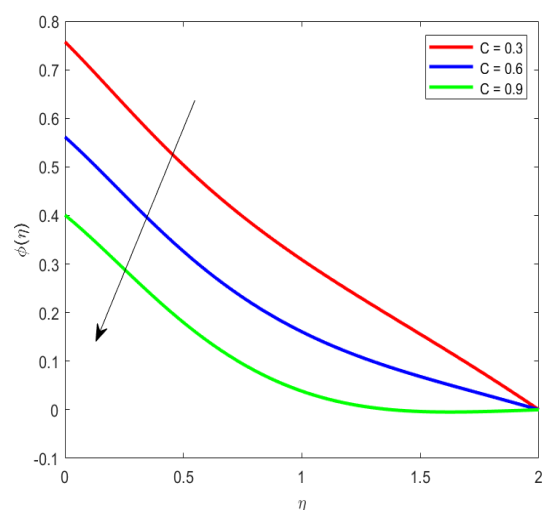


Fig. 10. Variations in $\phi(\eta)$ against C

The velocity field $f'(\eta)$ is affected by the magnetic parameter M , as seen in Figure 11. It is discovered that a decrease in fluid velocity was taken by an increase in the magnetic parameter. This is because, as illustrated in Figures 12 and 13, when a magnetic field is introduced, a drag force similar to the Lorentz force exists and appears as resistance to fluid flow. Due to the decreased fluid velocity, the temperature and concentration profiles are elevated.

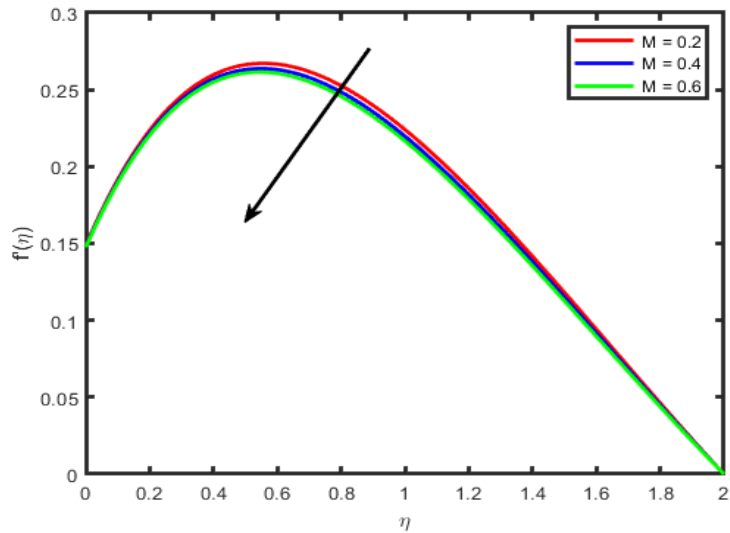


Fig. 11. Variations in $f'(\eta)$ against M

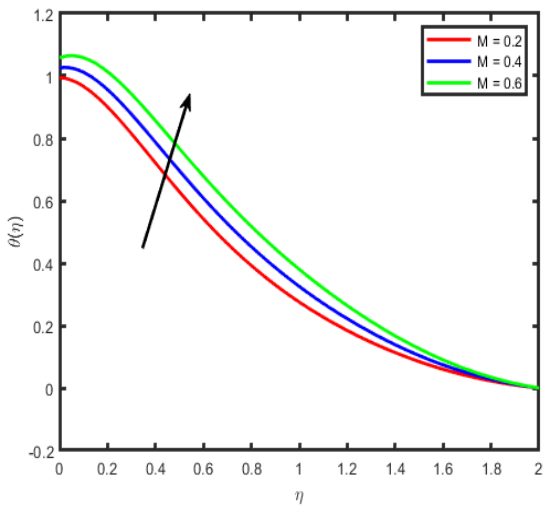


Fig. 12. Variations in $\theta(\eta)$ against M

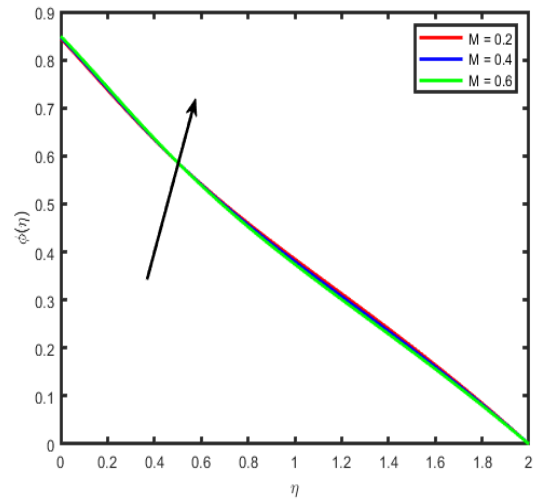


Fig. 13. Variations in $\phi(\eta)$ against M

Figures 14 and 17 depict how the thermal Grashof number (G_c) and concentration Grashof number (G_r) affect the velocity profile. It has been discovered that increasing the temperature and concentration of Grashof parameters induces an increase in the velocity profile. This is because a greater Grashof number produces a larger buoyant force, which leads to more fluid movement. Figures 18 and 19 show, respectively, how the Grashof number affects the temperature and concentration curves. The viscous force decreases as the solutal Grashof number rises, lowering the fluid's temperature and concentration. Similar to this, Figure 15 and 16 demonstrates that the temperature and concentration profiles falls as the thermal Grashof number rises.

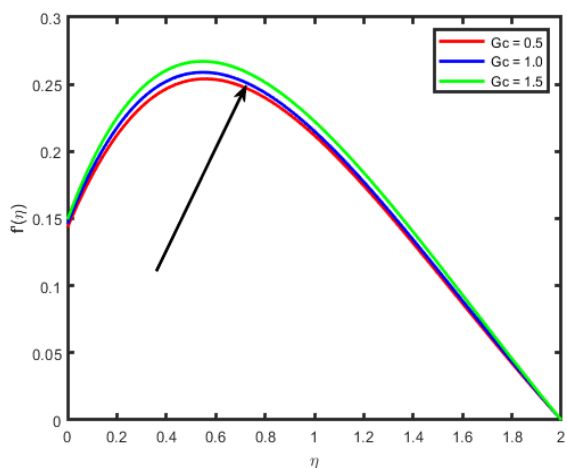


Fig. 14. Variations in $f'(\eta)$ against Gc

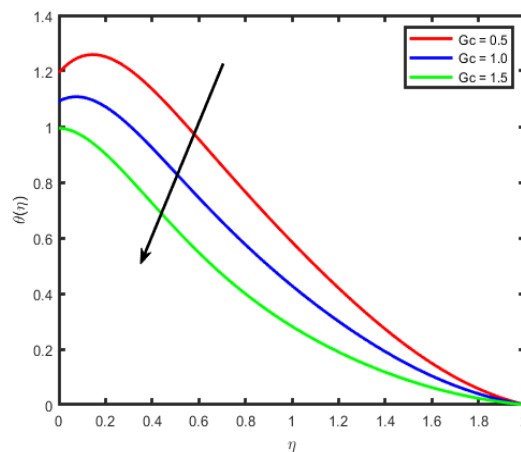


Fig. 15. Variations in $\theta(\eta)$ against Gc

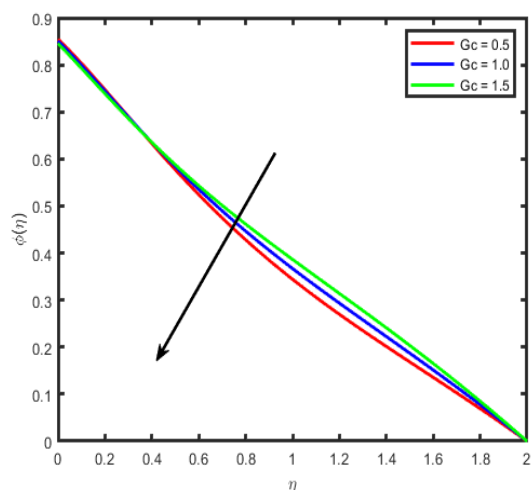


Fig. 16. Variations in $\phi(\eta)$ against Gc

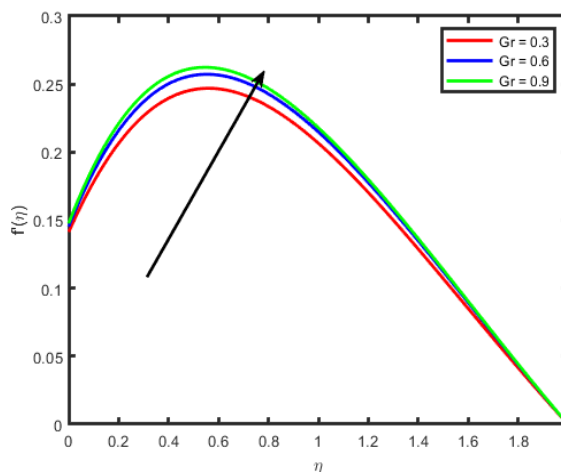


Fig. 17. Variations in $f'(\eta)$ against Gr

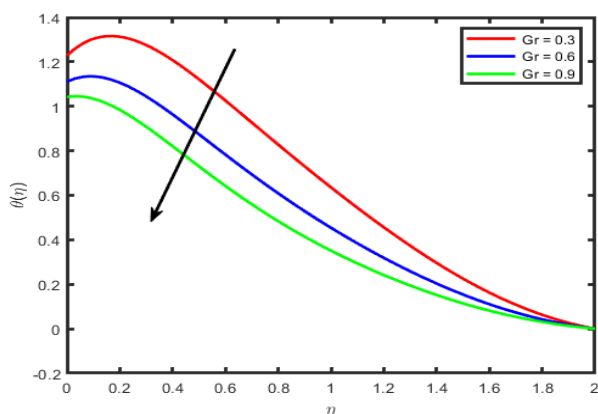


Fig. 18. Variations in $\theta(\eta)$ against Gr

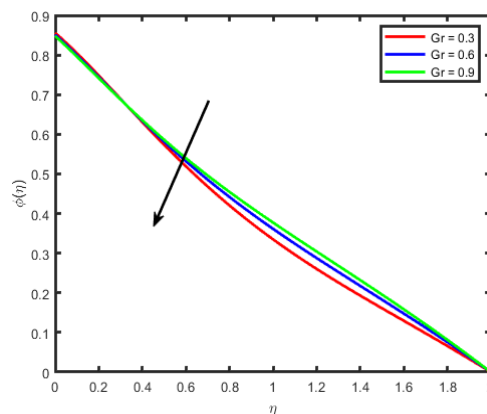


Fig. 19. Variations in $\phi(\eta)$ against Gr

Figure 20 illustrates how the Schmidt number (Sc) affects mass transfer. It is clear that a rising Schmidt number results in a declining concentration profile. This is explained by the fact that when the diffusion coefficient rises, the rate of mass transfer decreases, lowering the concentration profile.

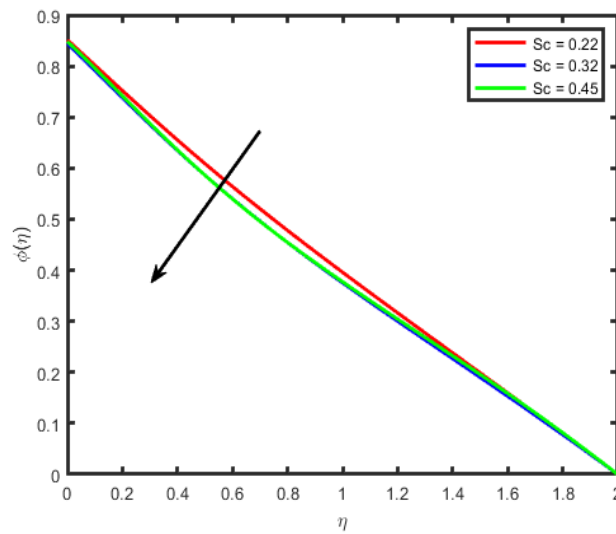


Fig. 20. Variations in $\phi(\eta)$ against Sc

Figure 21 depicts the impact of the chemical reactant factor Kr on the concentration profile. The hybrid nanofluid flow's concentration profile is decreased by the greater chemical reaction factor.

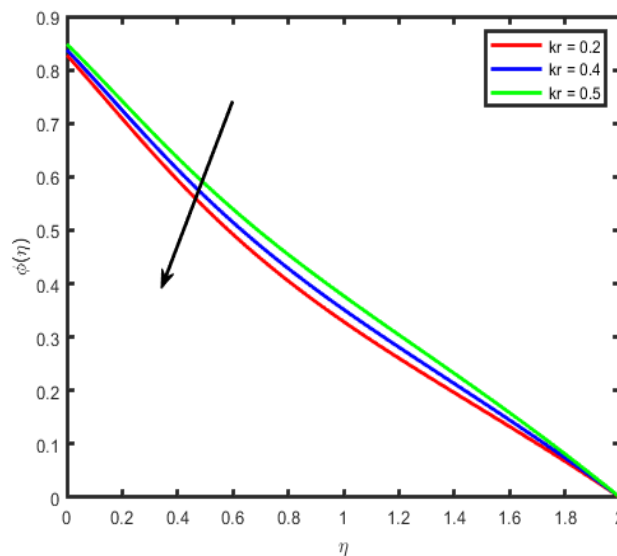


Fig. 21. Variations in $\phi(\eta)$ against Kr

Figure 22 demonstrates the influence of the heat source term (Q) on the thermal behaviour of the Ag-CuO/blood hybrid nanofluid. It is observed that the presence of the heat source term accelerates the thermal trend of the fluid flow. The heat generation and absorption terms act as a healing agent, directly affecting the energy profile.

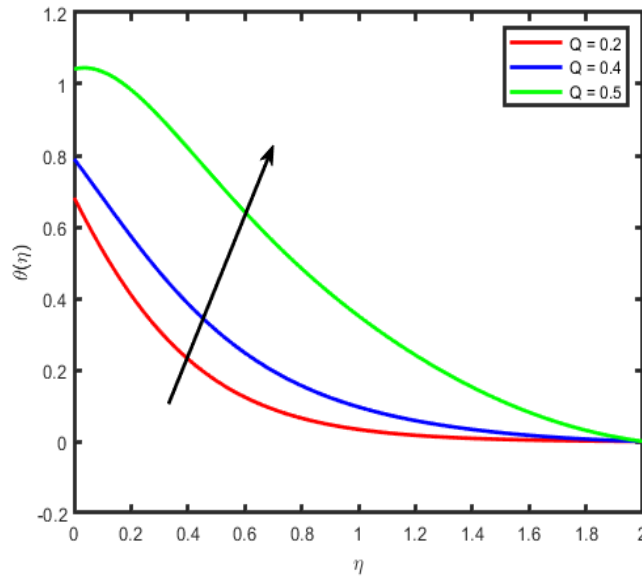


Fig. 22. Variations in $\theta(\eta)$ against Q

The fluctuations in the skin friction $C_f Re_x^{-1/2}$ are shown in Table 3, and it is evident that as the magnetic parameter M and the velocity slip parameter a rise, the skin friction tends to fall. Table 4 & 5 represents the numerical values of local Nusselt number and Sherwood number for different parameters. In table 6, the accuracy of the calculations being made is ensured by comparing them to the research done by Abdul Samad Khan *et al.*, [14]. From this table, it is clear that there is an outstanding agreement.

Table 3

Numerical values of skin friction coefficient when M=0.2, S=0.5, Gr=0.3, Gc=0.5

M	λ	A	S	Gr	Gc	$-C_f Re_x^{1/2}$
0.2						-0.117325
0.4						-0.114672
0.6						-0.111276
	0.4					-0.110286
	0.5					-0.113244
	0.6					-0.114625
		0.2				-0.113269
		0.4				-0.110258
		0.6				-0.100289
			0.5			-0.16288
			0.6			-0.14625
			0.7			-0.12628
				0.3		-0.10268
				0.6		-0.11429
				0.9		-0.1528
					0.5	-0.10228
					1.0	-0.11268
					1.5	-0.11564

Table 4
 Numerical values of the local Nusselt number $Nu_x Re_x^{-1/2}$ when $Pr = 0.7, B = 0.3, Q = 0.2, h = -0.3$

Pr	B	Q	$Nu_x Re_x^{-1/2}$
0.7		0.2	0.42869
0.8			0.44264
0.9			0.47086
	0.3		0.46264
	0.6		0.45209
	0.9		0.45260
		0.4	0.46264
		0.5	0.45206

Table 5
 Numerical values of Sherwood number for different parameters

Sc	Kr	$Sh_x Re_x^{-1/2}$
0.22	0.2	0.32684
0.32		0.31206
0.45		0.29004
	0.4	0.46284
	0.5	0.44001

Table 6
 Comparison of numerical solution with Khan *et al.*, [14] for $\theta(\eta)$ at $Gr=0, Gc=0, Sc=0, Kr=0$

η	Present value	Abdul Samad <i>et al.</i> , [14]	Absolute error
0.0	0.943155	0.942573	0.000582
0.5	0.882399	0.881382	0.001017
1.0	0.813842	0.812507	0.001335

5. Conclusions

The current study presents several noteworthy contributions in comparison to existing literature. The methodology employed in this work introduces several innovative aspects that distinguish it from previous studies.

- i. The temperature and concentration rise as the magnetic parameter (M) is amplified, but the velocity falls.
- ii. Skin friction increases with higher values of the magnetic and velocity slip parameters, indicating a decrease in fluid velocity.
- iii. A drop in the concentration profile results from a rise in the Schmidt number.
- iv. The temperature distribution grows with increasing heat generation parameters but drops with higher thermal slip and mass transfer parameters, while the Nusselt number decreases with higher thermal slip and heat production parameters.
- v. Table 4 showcases an insightful correlation between the rate of heat transfer and the Prandtl numbers (Pr). It demonstrates decreases in the rate of heat transfer with increasing B and Q, while an increase is observed as Prandtl numbers are elevated.

- vi. Table 5 demonstrates that the Sherwood number decreases significantly with the Schmidt number.

Acknowledgement

This research was not funded by any grant

References

- [1] Choi, S. US, and Jeffrey A. Eastman. *Enhancing thermal conductivity of fluids with nanoparticles*. No. ANL/MSD/CP-84938; CONF-951135-29. Argonne National Lab.(ANL), Argonne, IL (United States), 1995.
- [2] Ramzan, Muhammad, Naila Shaheen, Jae Dong Chung, Seifedine Kadry, Yu-Ming Chu, and Fares Howari. "Impact of Newtonian heating and Fourier and Fick's laws on a magnetohydrodynamic dusty Casson nanofluid flow with variable heat source/sink over a stretching cylinder." *Scientific Reports* 11, no. 1 (2021): 2357. <https://doi.org/10.1038/s41598-021-81747-x>
- [3] Hayat, Tanzila, and S. Nadeem. "Heat transfer enhancement with Ag–CuO/water hybrid nanofluid." *Results in physics* 7 (2017): 2317-2324. <https://doi.org/10.1016/j.rinp.2017.06.034>
- [4] Waini, Iskandar, Anuar Ishak, and Ioan Pop. "Unsteady flow and heat transfer past a stretching/shrinking sheet in a hybrid nanofluid." *International Journal of Heat and Mass Transfer* 136 (2019): 288-297. <https://doi.org/10.1016/j.ijheatmasstransfer.2019.02.101>
- [5] Waini, Iskandar, Anuar Ishak, and Ioan Pop. "Flow and heat transfer along a permeable stretching/shrinking curved surface in a hybrid nanofluid." *Physica Scripta* 94, no. 10 (2019): 105219. <https://doi.org/10.1088/1402-4896/ab0fd5>
- [6] Waini, Iskandar, Anuar Ishak, and Ioan Pop. "Hybrid nanofluid flow and heat transfer over a nonlinear permeable stretching/shrinking surface." *International Journal of Numerical Methods for Heat & Fluid Flow* 29, no. 9 (2019): 3110-3127. <https://doi.org/10.1108/HFF-01-2019-0057>
- [7] Waini, Iskandar, Anuar Ishak, and Ioan Pop. "Hybrid nanofluid flow and heat transfer past a vertical thin needle with prescribed surface heat flux." *International Journal of Numerical Methods for Heat & Fluid Flow* 29, no. 12 (2019): 4875-4894. <https://doi.org/10.1108/HFF-04-2019-0277>
- [8] Waini, Iskandar, Anuar Ishak, and Ioan Pop. "Transpiration effects on hybrid nanofluid flow and heat transfer over a stretching/shrinking sheet with uniform shear flow." *Alexandria Engineering Journal* 59, no. 1 (2020): 91-99. <https://doi.org/10.1016/j.aej.2019.12.010>
- [9] Waini, Iskandar, Anuar Ishak, and Ioan Pop. "Hybrid nanofluid flow induced by an exponentially shrinking sheet." *Chinese Journal of Physics* 68 (2020): 468-482. <https://doi.org/10.1016/j.cjph.2019.12.015>
- [10] Hayat, Tanzila, S. Nadeem, and A. U. Khan. "Rotating flow of Ag-CuO/H₂O hybrid nanofluid with radiation and partial slip boundary effects." *The European Physical Journal E* 41 (2018): 1-9. <https://doi.org/10.1140/epje/i2018-11682-y>
- [11] Chamkha, Ali J., Igor V. Miroshnichenko, and Mikhail A. Sheremet. "Numerical analysis of unsteady conjugate natural convection of hybrid water-based nanofluid in a semicircular cavity." *Journal of Thermal Science and Engineering Applications* 9, no. 4 (2017): 041004. <https://doi.org/10.1115/1.4036203>
- [12] Hayat, Tanzila, and S. Nadeem. "Heat transfer enhancement with Ag–CuO/water hybrid nanofluid." *Results in physics* 7 (2017): 2317-2324. <https://doi.org/10.1016/j.rinp.2017.06.034>
- [13] Andersson, Helge I., Olav R. Hansen, and Bjørn Holmedal. "Diffusion of a chemically reactive species from a stretching sheet." *International Journal of Heat and Mass Transfer* 37, no. 4 (1994): 659-664. [https://doi.org/10.1016/0017-9310\(94\)90137-6](https://doi.org/10.1016/0017-9310(94)90137-6)
- [14] Khan, Abdul Samad, He-Yong Xu, and Waris Khan. "Magnetohydrodynamic hybrid nanofluid flow past an exponentially stretching sheet with slip conditions." *Mathematics* 9, no. 24 (2021): 3291. <https://doi.org/10.3390/math9243291>
- [15] Chamkha, Ali J., Igor V. Miroshnichenko, and Mikhail A. Sheremet. "Numerical analysis of unsteady conjugate natural convection of hybrid water-based nanofluid in a semicircular cavity." *Journal of Thermal Science and Engineering Applications* 9, no. 4 (2017): 041004. <https://doi.org/10.1115/1.4036203>
- [16] Khan, Umair, Iskandar Waini, Aurang Zaib, Anuar Ishak, and Ioan Pop. "MHD mixed convection hybrid nanofluids flow over a permeable moving inclined flat plate in the presence of thermophoretic and radiative heat flux effects." *Mathematics* 10, no. 7 (2022): 1164. <https://doi.org/10.3390/math10071164>
- [17] Kumar, T. Sravan. "Hybrid nanofluid slip flow and heat transfer over a stretching surface." *Partial Differential Equations in Applied Mathematics* 4 (2021): 100070. <https://doi.org/10.1016/j.padiff.2021.100070>

- [18] Roy, Nepal Chandra, Anwar Hossain, and Ioan Pop. "Flow and heat transfer of MHD dusty hybrid nanofluids over a shrinking sheet." *Chinese Journal of Physics* 77 (2022): 1342-1356. <https://doi.org/10.1016/j.cjph.2021.12.012>
- [19] Khashi'ie, Najiyah Safwa, Ezad Hafidz Hafidzuddin, Norihan Md Arifin, and Nadiah Wah. "Stagnation point flow of hybrid nanofluid over a permeable vertical stretching/shrinking cylinder with thermal stratification effect." *CFD Letters* 12, no. 2 (2020): 80-94.
- [20] Sulochana, C., and Geeta C. Shivapuji. "Numerical Analysis of Hybrid Nanofluid Flow Over a Nonlinear Stretching Sheet with Viscous Dissipation, Joule Heating Effects." *CFD Letters* 14, no. 10 (2022): 42-55. <https://doi.org/10.37934/cfdl.14.10.4255>
- [21] Awais, Muhammad, Tasawar Hayat, Sania Irum, and Ahmed Alsaedi. "Heat generation/absorption effects in a boundary layer stretched flow of Maxwell nanofluid: Analytic and numeric solutions." *PLoS one* 10, no. 6 (2015): e0129814. <https://doi.org/10.1371/journal.pone.0129814>
- [22] Ahmad Khan, Junaid, M. Mustafa, T. Hayat, and A. Alsaedi. "Numerical study of Cattaneo-Christov heat flux model for viscoelastic flow due to an exponentially stretching surface." *PLOS one* 10, no. 9 (2015): e0137363. <https://doi.org/10.1371/journal.pone.0137363>
- [23] Mustafa, Meraj, Ammar Mushtaq, Tasawar Hayat, and Bashir Ahmad. "Nonlinear radiation heat transfer effects in the natural convective boundary layer flow of nanofluid past a vertical plate: a numerical study." *PLoS One* 9, no. 9 (2014): e103946. <https://doi.org/10.1371/journal.pone.0103946>
- [24] Mushtaq, A., M. Mustafa, T. Hayat, and A. Alsaedi. "Numerical study of the non-linear radiation heat transfer problem for the flow of a second-grade fluid." *Bulg. Chem. Comm* 47, no. 2 (2015): 725-732.
- [25] Olajuwon, B. I. "Convection heat and mass transfer in a hydromagnetic flow of a second grade fluid in the presence of thermal radiation and thermal diffusion." *International Communications in Heat and Mass Transfer* 38, no. 3 (2011): 377-382. <https://doi.org/10.1016/j.icheatmasstransfer.2010.11.006>
- [26] Bestman, A. R. "Natural convection boundary layer with suction and mass transfer in a porous medium." *International journal of energy research* 14, no. 4 (1990): 389-396. <https://doi.org/10.1002/er.4440140403>
- [27] Tayebi, Tahar, and Ali J. Chamkha. "Entropy generation analysis during MHD natural convection flow of hybrid nanofluid in a square cavity containing a corrugated conducting block." *International Journal of Numerical Methods for Heat & Fluid Flow* 30, no. 3 (2019): 1115-1136. <https://doi.org/10.1108/HFF-04-2019-0350>
- [28] Takabi, Behrouz, and Saeed Salehi. "Augmentation of the heat transfer performance of a sinusoidal corrugated enclosure by employing hybrid nanofluid." *Advances in Mechanical Engineering* 6 (2014): 147059. <https://doi.org/10.1155/2014/147059>
- [29] Oztop, Hakan F., and Eiyad Abu-Nada. "Numerical study of natural convection in partially heated rectangular enclosures filled with nanofluids." *International journal of heat and fluid flow* 29, no. 5 (2008): 1326-1336. <https://doi.org/10.1016/j.ijheatfluidflow.2008.04.009>
- [30] Na, Tsung Yen, ed. *Computational methods in engineering boundary value problems*. Academic press, 1980.